Electronic Supplementary Material (ESI) for Nanoscale.

Probing Ca^{2+}-induced conformational change of Calmodulin with gold nanoparticle-decorated single-walled carbon nanotube field-effect transistors

Wenting Shao[†], Seth C. Burkert[†], David L. White[†], Valerie L. Scott[†], Jianfu Ding[‡], Zhao Li[‡], Jianying Ouyang[‡], Francois Lapointe[‡], Patrick R. L. Malenfant[‡], Kabirul Islam[†], Alexander Star[†]*

[†] Department of Chemistry, University of Pittsburgh, Pittsburgh, Pennsylvania 15260, United States

[‡] Security and Disruptive Technologies Portfolio, National Research Council Canada, 1200 Montreal Road, Ottawa, Ontario, K1A 0R6, Canada

Table of Contents

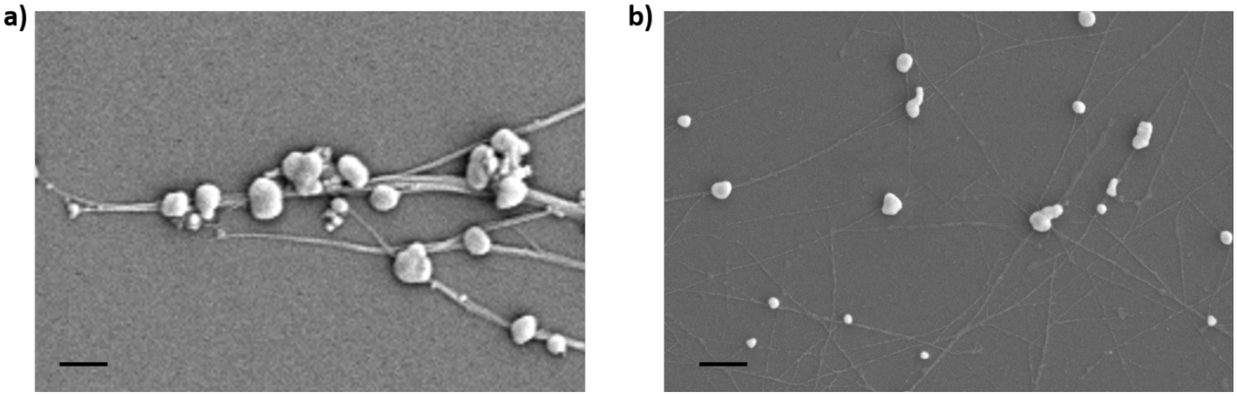

Figure S1. SEM images of a) AuNPs decorated un-SWCNTs and b) AuNPs decorated sc-SWCNTs. Both SEM images show an area of 1578 nm X 2353 nm on the device surface. It can be observed that less un-SWCNTs were deposited on the substrate than sc-SWCNT, indicating that sc-SWCNT formed denser networks than un-SWCNTs. (Scale bar: a) 200 nm; b) 200 nm)

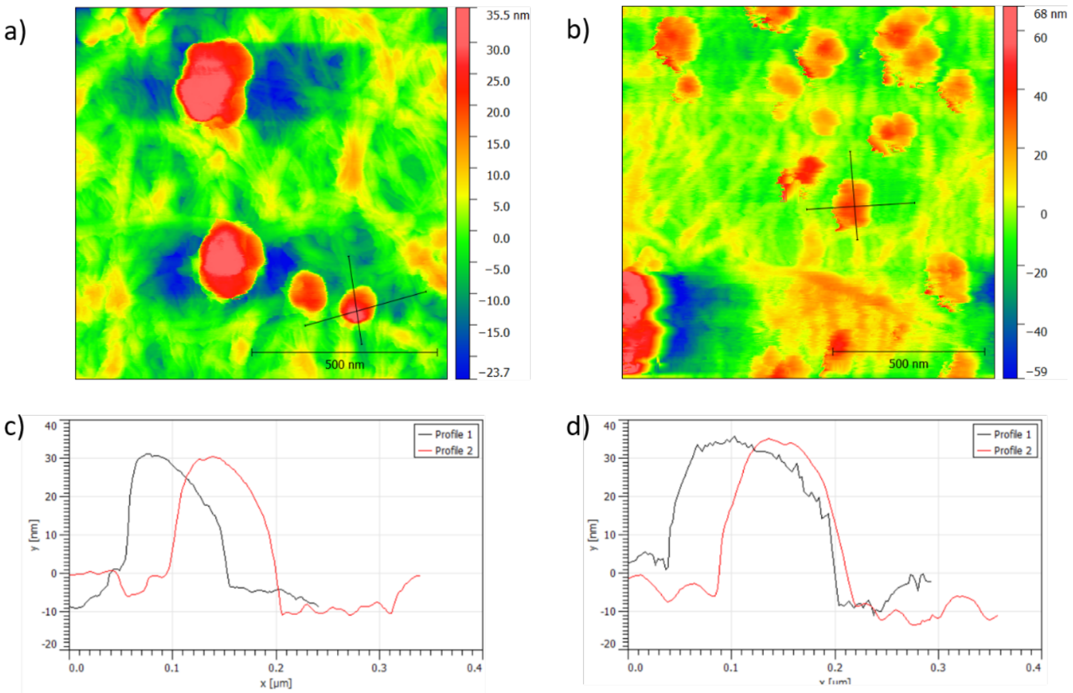

Figure S2. a) Atomic force microscopy (AFM) image of AuNP decorated sc-SWCNTs. b) AFM image of Au-SWCNTs after CaM binding. c) Height profile of Au-sc-SWCNTs. d) Height profile of CaM-Au-sc-SWCNTs.

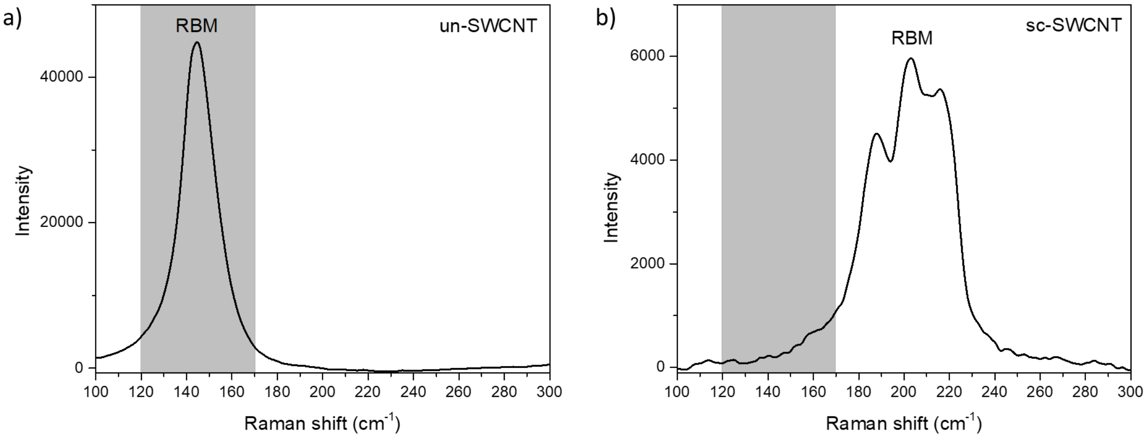

Figure S3. RBM peaks of a) un-SWCNT and b) sc-SWCNT under 785 nm laser excitation. Peaks in the shaded area from 120 cm^{-1} to 170 cm^{-1} are associated with the metallic features of SWCNTs. un-SWCNT has an RBM peak centered around 145 cm^{-1}. In contrast, this peak is absent in sc-SWCNT, a broad and splitting RBM peak arises at 204 cm^{-1} instead. This result confirms the high purity content of sc-SWCNT.[S1-S3]

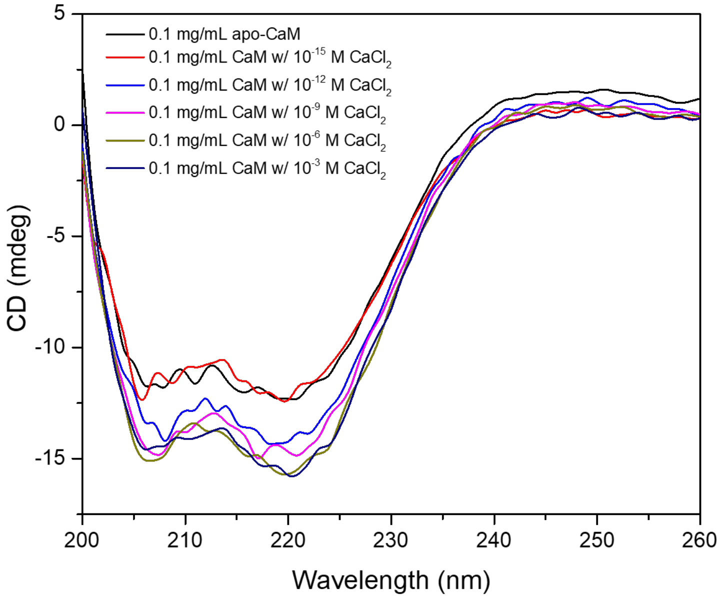

Figure S4. Circular Dichroism solution spectra of calcium-free CaM (apo-CaM) and calcium-bound CaM with different concentrations of $CaCl_2$.

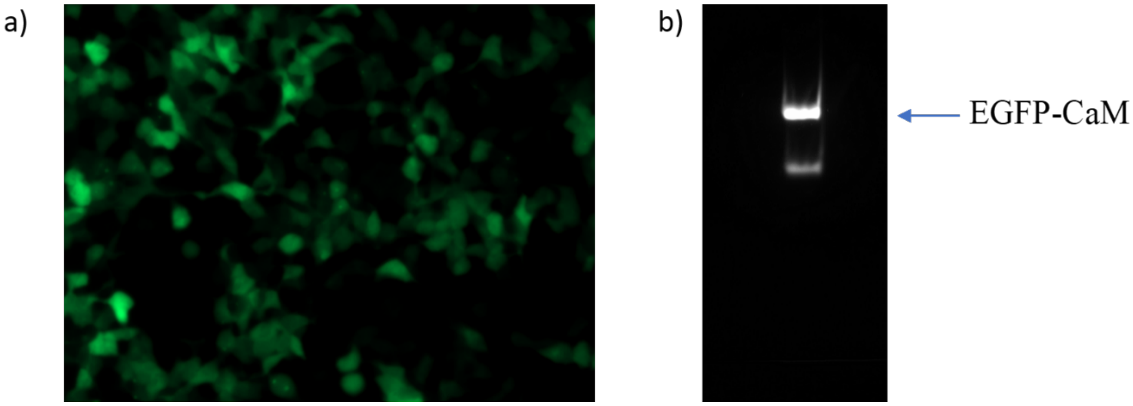

Figure S5. a) Successful expression of EGFP-CaM in HEK293T cells was confirmed by live-cell imaging using Zeiss microscope. b) In-gel fluorescence showing purified EGFP-CaM protein.

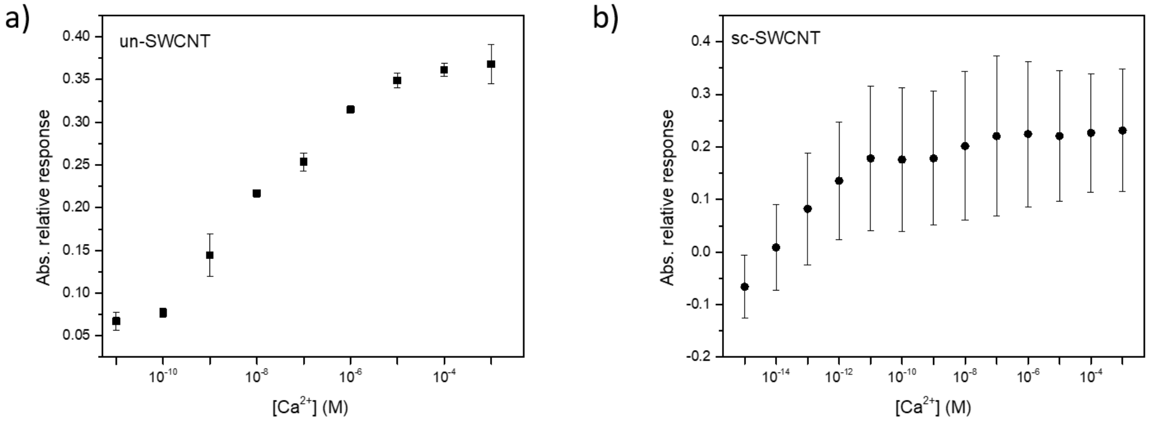

Figure S6. Device reproducibility of a) un-SWCNT and b) sc-SWCNT FET devices. For both types of devices, the calibration curve was constructed by plotting the averaged relative conductance changes from multiple devices at – 0.5 V_g against concentrations of Ca^{2+} solution. Error bars were calculated from 4 different devices for un-SWCNT devices, and 5 different devices for sc-SWCNT devices. The larger error bars for sc-SWCNT devices suggest larger device-to-device variations for sc-SWCNT devices.

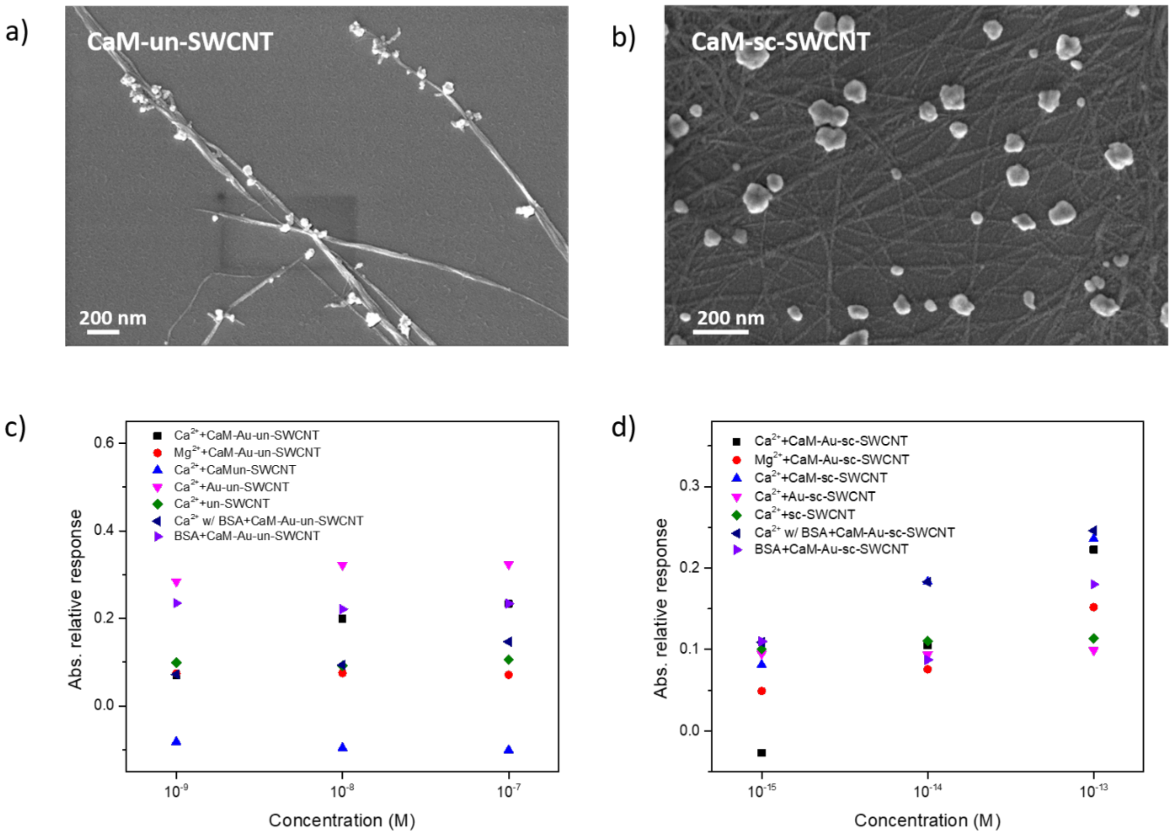

Figure S7. a) SEM image of CaM on un-SWCNT networks. b) SEM image of CaM on sc-SWCNT networks. c) Calibration plot of the active system and control systems of un-SWCNT FET devices. d) Calibration plot of the active system and control systems of sc-SWCNT FET devices in the corresponding linear range.

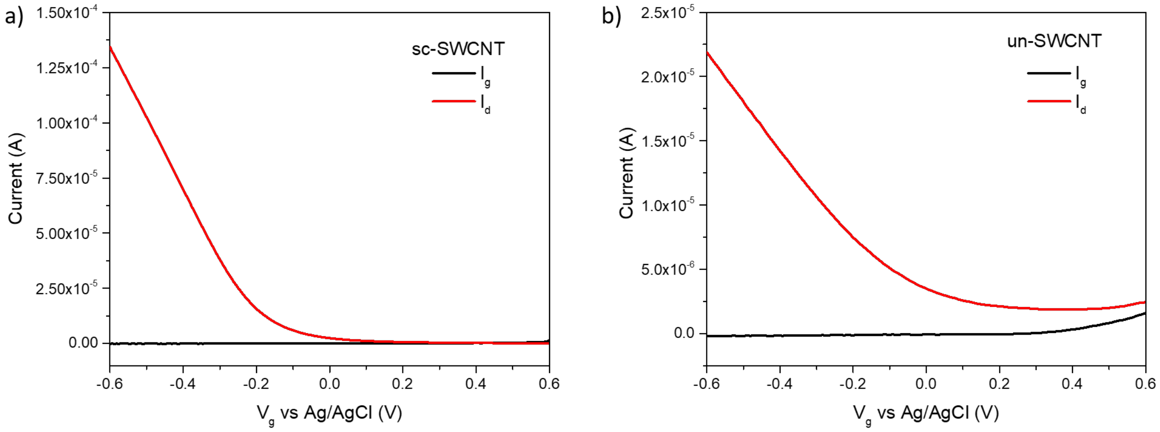

Figure S8. Comparison of source-drain current (I_d) and gate leakage current (I_g) for a) sc-SWCNT and b) un-SWCNT FET devices. The gate current is insignificant compared to the source-drain current, therefore the effect of leakage current is negligible.

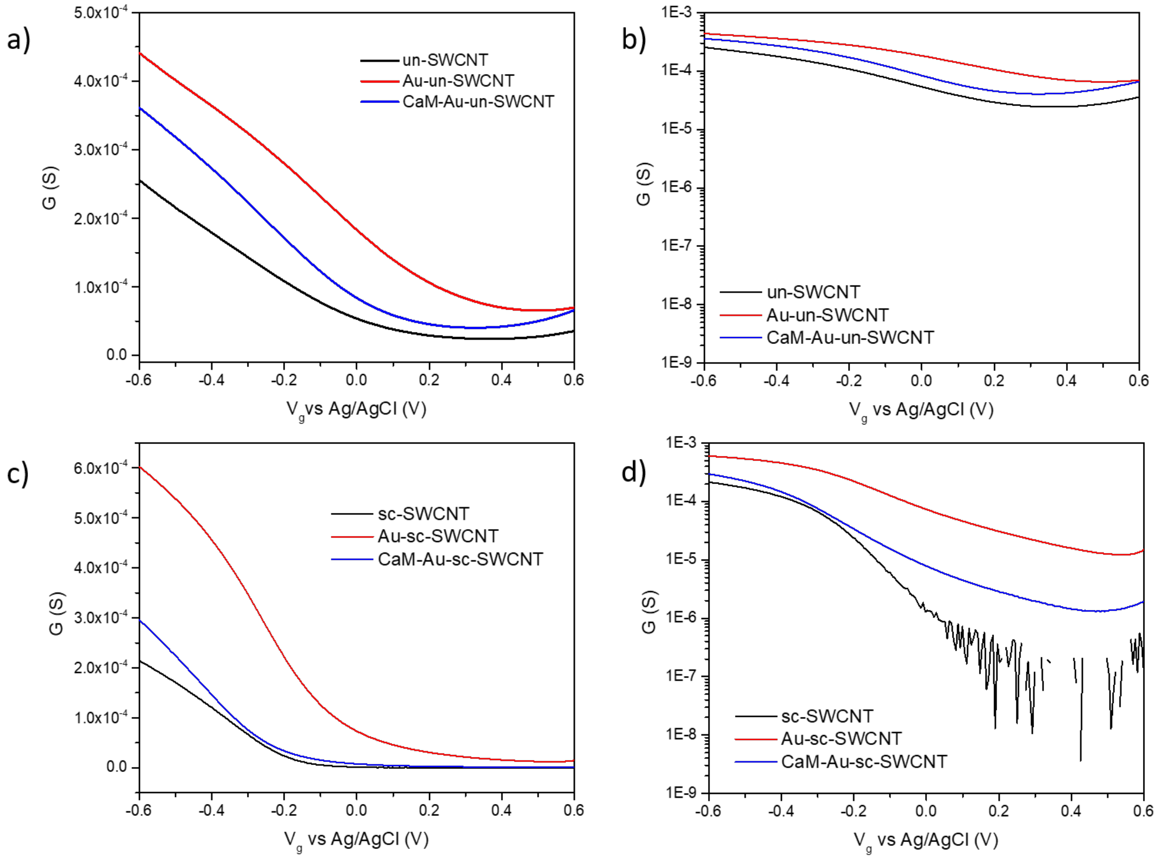

Figure S9. a) FET characteristic curves of CaM-Au-un-SWCNT FET device during each step of functionalization plotting in linear scale and b) logarithmic scale. c) FET characteristic curves of CaM-Au-sc-SWCNT FET device during each step of functionalization plotting in linear scale and d) logarithmic scale. The on/off ratio of un-SWCNT FET device was ~3, while the on/off ratio of sc-SWCNT FET device was ~10^4. sc-SWCNT FET devices show better on/off ratio due to the lack of metallic carbon nanotubes, therefore efficiently turning off the device.

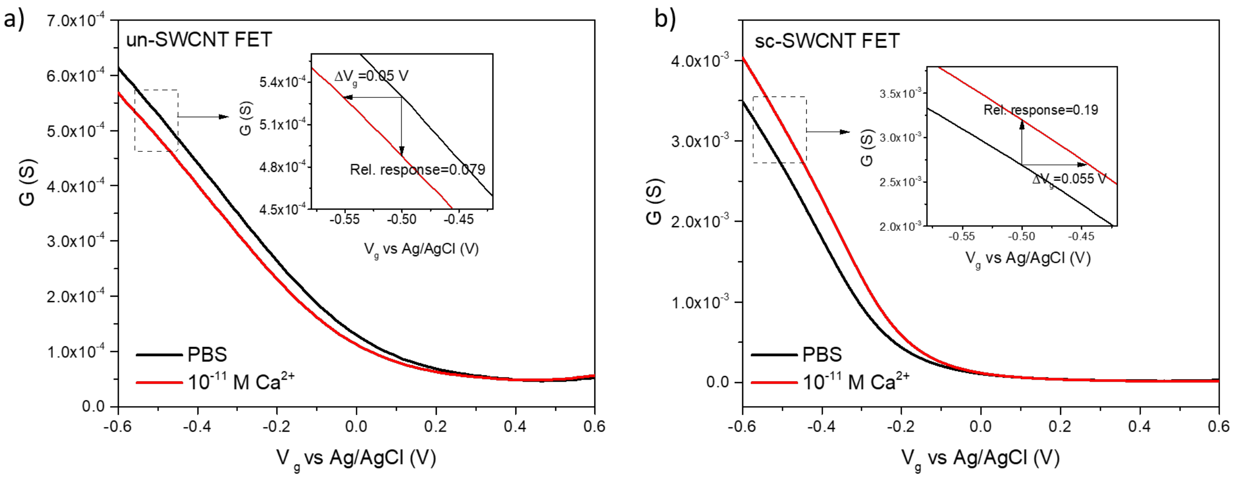

Figure S10. Absolute relative response of a) CaM-Au-un-SWCNT FET device and b) CaM-Au-sc-SWCNT FET device to 10^{-11} M Ca^{2+}. With higher on/off ratio, sc-SWCNT FET device had a significant higher absolute relative response than un-SWCNT FET device, even though the shift of gate voltage was similar.

Table S1. Comparison of various methods for Ca^{2+} detection

Ca^{2+} detection method	**Ca^{2+} detection limit**	**Reference in the main text**
Ca^{2+} selective PVC-membrane electrode	7.5×10^{-7} M	61
Solid-contact Ca^{2+} selective electrode	(3.4-8.2) $\times 10^{-6}$ M	62
$NiCo_2O_4$/3-D Graphene	0.38 μM	63
Fluorescent carbon quantum dot	77 pM (in human serum)	64
CaM-Au-sc-SWCNT FET	10^{-15} M	This work

References

S1. Ding, J.; Li, Z.; Lefebvre, J.; Cheng, F.; Dunford, J. L.; Malenfant, P. R.; Humes, J.; Kroeger, J., A hybrid enrichment process combining conjugated polymer extraction and silica gel adsorption for high purity semiconducting single-walled carbon nanotubes (SWCNT). *Nanoscale* **2015,** *7*, 15741–15747.

S2. Li, Z.; Ding, J.; Finnie, P.; Lefebvre, J.; Cheng, F.; Kingston, C. T.; Malenfant, P. R. L., Raman microscopy mapping for the purity assessment of chirality enriched carbon nanotube networks in thin-film transistors. *Nano Res.* **2015,** *8*, 2179–2187.

S3. Ding, J.; Li, Z.; Lefebvre, J.; Cheng, F.; Dubey, G.; Zou, S.; Finnie, P.; Hrdina, A.; Scoles, L.; Lopinski, G. P.; Kingston, C. T.; Simard, B.; Malenfant, P. R., Enrichment of large-diameter semiconducting SWCNTs by polyfluorene extraction for high network density thin film transistors. *Nanoscale* **2014,** *6*, 2328–2339.